Acta Pharmaceutica Sinica B 2024;14(11):5026–5036

Chinese Pharmaceutical Association
Institute of Materia Medica, Chinese Academy of Medical Sciences

Acta Pharmaceutica Sinica B

www.elsevier.com/locate/apsb
www.sciencedirect.com

ORIGINAL ARTICLE

Immunometabolic rewiring in macrophages for periodontitis treatment *via* nanoquercetin-mediated leverage of glycolysis and OXPHOS

Yi Zhang[a,b,†], Junyu Shi[a,†], Jie Zhu[b], Xinxin Ding[a], Jianxu Wei[a], Xue Jiang[a], Yijie Yang[a], Xiaomeng Zhang[a,*], Yongzhuo Huang[b,c,d,*], Hongchang Lai[a,*]

[a]*Department of Implant Dentistry, Shanghai Ninth People's Hospital, Shanghai Jiao Tong University School of Medicine, College of Stomatology, Shanghai Jiao Tong University, National Center for Stomatology, National Clinical Research Center for Oral Diseases, Shanghai Key Laboratory of Stomatology, Shanghai 200011, China*
[b]*State Key Laboratory of Drug Research, Shanghai Institute of Materia Medica, Chinese Academy of Sciences, Shanghai 201203, China*
[c]*Zhongshan Institute for Drug Discovery, Shanghai Institute of Materia Medica, Chinese Academy of Sciences, Zhongshan 528437, China*
[d]*NMPA Key Laboratory for Quality Research and Evaluation of Pharmaceutical Excipients, Shanghai 201203, China*

Received 21 March 2024; received in revised form 28 May 2024; accepted 15 June 2024

KEY WORDS

Quercetin;
Periodontitis;
Macrophage;
Glycolysis;
Oxidative phosphorylation (OXPHOS);
Mesoporous polydopamine;
Mitochondrial reactive oxygen species;

Abstract Periodontitis is a chronic inflammatory disease marked by a dysregulated immune microenvironment, posing formidable challenges for effective treatment. The disease is characterized by an altered glucose metabolism in macrophages, specifically an increase in aerobic glycolysis, which is linked to heightened inflammatory responses. This suggests that targeting macrophage metabolism could offer a new therapeutic avenue. In this study, we developed an immunometabolic intervention using quercetin (Q) encapsulated in bioadhesive mesoporous polydopamine (Q@MPDA) to treat periodontitis. Our results demonstrated that Q@MPDA could reprogram inflammatory macrophages to an anti-inflammatory phenotype (*i.e.*, from-M1-to-M2 repolarization). In a murine periodontitis model, locally administered Q@MPDA reduced the presence of inflammatory macrophages, and decreased the levels of inflammatory cytokines (IL-1β and TNF-α) and reactive oxygen species (ROS) in the periodontium.

*Corresponding authors.
E-mail addresses: 119039@sh9hospital.org.cn (Xiaomeng Zhang), yzhuang@simm.ac.cn (Yongzhuo Huang), laihongchang@sjtu.edu.cn (Hongchang Lai).
[†]These authors made equal contributions to this work.

Peer review under the responsibility of Chinese Pharmaceutical Association and Institute of Materia Medica, Chinese Academy of Medical Sciences.

https://doi.org/10.1016/j.apsb.2024.07.008

Immunometabolic rewiring

Consequently, it alleviated periodontitis symptoms, reduced alveolar bone loss, and promoted tissue repair. Furthermore, our study revealed that Q@MPDA could inhibit the glycolysis of inflammatory macrophages while enhancing oxidative phosphorylation (OXPHOS), facilitating the shift from M1 to M2 macrophage subtype. Our findings suggest that Q@MPDA is a promising treatment for periodontitis *via* immunometabolic rewiring.

1. Introduction

Cellular metabolism plays a crucial role in shaping cell functions, with metabolic patterns adapting to microenvironment changes in various pathologic conditions[1]. As a result, metabolic modulation—particularly glycolysis inhibition and oxidative phosphorylation promotion—has become a novel therapeutic strategy for a range of diseases, including metabolic, cardiovascular, inflammatory disorders, and orthopedic conditions[2,3]. For example, macrophage glucose metabolism is closely related to inflammation regulation. Aerobic glycolysis is upregulated by inflammatory signals, whereas oxidative phosphorylation (OXPHOS) is associated with an anti-inflammatory pattern[4]. Therefore, targeting macrophage glucose metabolism holds promise for treating inflammatory diseases.

Traditional periodontitis treatment typically involves mechanical debridement and antibiotic therapy. However, it often falls short in case of refractory periodontitis due to underlying immune dysregulation[5]. An increased presence of pro-inflammatory M1 macrophages leads to the secretion of pro-inflammatory cytokines, tissue destruction, and hinders healing processes[6]. Thereby, dysfunctional macrophage-mediated chronic inflammation renders periodontitis hard to cure. The metabolic profiles of pro- and anti-inflammatory macrophages are distinct, with M1 favoring glycolysis and M2 favoring OXPHOS[7]. It is expected that targeting glycolysis in the inflammatory macrophages is a potential therapeutic strategy for periodontitis.

Quercetin, a common dietary flavanol known for its anti-inflammatory and anti-oxidative effects, has been explored for periodontitis management[8,9]. While its effect on glycolysis inhibition has been demonstrated in cancer cells and platelets for anti-cancer treatment[10–12], its role in regulating glucose metabolism in pro-inflammatory macrophages remained underexplored. However, quercetin for periodontitis application is impeded by its low solubility, chemical instability, and poor drug retention due to continuous saliva flow in the oral cavity. These limitations necessitate an effective drug delivery system. Mesoporous polydopamine (MPDA), an organic mesoporous nanocarrier, is ideal for local delivery due to its biocompatibility, adhesive properties, and functionalized surface area[13]. MPDA's structure is particularly suitable for intragingival drug delivery; it can enable sustained release while countering salivary clearance and ensuring retention within the gingival sulcus. Moreover, MPDA can respond to the acidic conditions of inflamed tissues to control drug release.

In this study, we used MPDA to encapsulate quercetin to enhance its intragingival bioavailability and enable targeted modulation of macrophage metabolism. We investigated the effects of quercetin-loaded MPDA on glycolysis and OXPHOS in macrophages, and accessed the repolarization from the M1 (pro-inflammatory) to M2 (anti-inflammatory) phenotype. This study aims to develop a novel periodontitis treatment modality through immunometabolic regulation.

2. Materials and methods

2.1. Materials, cells, and animals

Quercetin and oligomycin A were purchased from Meilun Biotech Co., Ltd. (Dalian, China). Dulbecco's modified Eagle's Medium (DMEM), fetal bovine serum (Gibco®), and MitoSOX™ Red mitochondrial superoxide indicator for live-cell imaging were purchased from Thermo Fisher (Waltham, USA). Dialysis bag (MWCO 8−14K) was purchased from Yeasen Biotech Co., Ltd. (Shanghai, China) Dopamine hydrochloride, Pluronic® F127, lipopolysaccharide, Amicon® Ultra 3K device, and cocktail protease inhibitors, as well as 1,3,5-trimethyl benzene (TMB, 97%), were supplied by Sigma−Aldrich (St. Louis, USA). 2′,7′-Dichlorofluorescein diacetate (DCFH-DA) was purchased from Macklin Biochemical Co., Ltd. (Shanghai, China). Artificial saliva (ISO/TR10271, pH 6.8−7) and methylene blue hydrate were provided by Yuanye Biotech Co., Ltd. (Shanghai, China), and P.g-LPS was supplied by InvivoGen Co., Ltd. (San Diego, USA). Peprotech Co., Ltd. (Rocky Hill, USA) provided recombinant murine macrophage colony-stimulating factor (M-CSF), interferon-gamma (IFN-γ), and interleukin-4 (IL-4). Takara Biotech Co., Ltd. (Shiga, Japan) supplied the PrimeScript RT Reagent Kit and TB Green. Sango Biotech Co., Ltd. (Shanghai, China) supplied the primers. NcmECL Ultra was obtained by NCM Biotech Co., Ltd. (Suzhou, China) and Dakewe Biotech Co., Ltd. (Shanghai, China) supplied the ELISA kits. Beyotime Biotech Co., Ltd. (Shanghai, China) supplied the ROS assay kits, MitoTracker Red CMXRos, mitochondrial membrane potential assay kits with JC-1, DAPI, Hoechst 33342 stain solution, cell counting kit-8 (CCK-8), BCIP/NBT alkaline phosphatase color development kits, BCA protein assay kits, DAB, HRP-conjugated goat anti-rabbit/mouse lgG secondary antibody, and total antioxidant capacity assay kits with ABTS. Nanjing Jiancheng Bioengineering Institute (Nanjing, China) provided the Coenzyme INAD (H) content test kits, and TIANGEN Biotech Co., Ltd. (Beijing, China) supplied the TIANamp Genomic DNA kits. Solarbio Co., Ltd. (Beijing, China) provided glycero 2-phosphate disodium salt, dexamethasone, and ascorbic acid (Vitamin C). Coumarin 6 and other chemical reagents were provided by Sinopharm Chemical Reagent (Shanghai, China). ADP/ATP Ratio Assay Kit-Luminescence was provided by DOJINDO Laboratories Co., Ltd. (Kyushu, Japan).

Bone marrow-derived macrophages (BMDMs) and bone marrow-derived mesenchymal stem cells (BMSCs) were prepared from male C57BL/6 mice (4−6 weeks) obtained from the Shanghai Laboratory Animal Center (SLAC) Co., Ltd. (Shanghai, China) using standard

protocols[14]. BMSCs were cultured in a complete DMEM medium containing 20% FBS, while BMDMs were cultured in a DMEM medium supplemented with 30 ng/mL of M-CSF for four days. M1Φ was differentiated using LPS (100 ng/mL) and IFN-γ (20 ng/mL), and M2Φ using IL-4 (40 ng/mL). Murine fibroblast cells (L929) were cultured in a complete DMEM medium. L929 cells were obtained from the Shanghai Cell Bank of Chinese Academy of Sciences (Shanghai, China). The animal experiment protocol was approved by the Ethics Committee of Shanghai Institute of Materia Medica, Chinese Academy of Sciences (IACUC: 2021-07-HYZ-110).

2.2. Preparation and characterization of MPDA and quercetin-loaded MPDA (Q@MPDA)

MPDA nanoparticles were synthesized by a one-pot synthesis method[15], utilizing TMB as a template and F127 as a surfactant. F127 (1 g) was dissolved in 50 mL deionized water and mixed with 50 mL ethanol and 2 mL TMB solution with stirring. After 30 min, 0.5 g dopamine was added and fully mixed, followed by the addition of 5 mL ammonia for reaction. After 24 h, the MPDA NPs were purified by washing and then subjected to centrifugation in 50% ethanol, 12,000 rpm for 10 min (D1624R centrifuge, DLAB, Beijing, China), repeating three times.

For the Q@MPDA synthesis, 20 mg of MPDA was dissolved in 9 mL 50% ethanol and mixed with 5 mg of quercetin in 1 mL methanol at room temperature for 24 h. The suspension was purified using an Amicon® Ultra 3K device centrifugated at 4000×g for 15 min and then washed three times.

The Q@MPDA was characterized by a UV-vis spectrometer (Shimadzu, UV-1650PC, Kyoto, Japan), while the drug-loading capacity (DL%) and entrapment efficiency (EE%) were determined by HPLC (Agilent, Technologies 1260 Infinity, Santa Clara, USA). The size, zeta potential of MPDA and Q@MPDA were measured by dynamic light scattering analysis (Malvern Nano-ZS90, Malvern, UK). Morphology of MPDA and Q@MPDA was characterized by TEM (FEI, Tecnai G2 Spirit 120 KV, Hillsboro, USA), and SEM (ZEISS, Gemini 300, Oberkochen, Germany). Brunauer-Emmett-Teller (Quantachrome, Autosorb IQ3, Florida, USA) was used to characterize the specific surface area of MPDA and Q@MPDA. The antioxidant capacity was detected using an antioxidant capacity assay kit, and absorbance at 405 nm was measured.

2.3. Drug release experiment

Quercetin (0.05 mg/mL, 1 mL) and Q@MPDA (at an equal concentration of quercetin) were added to a dialysis bag (MWCO 8−14K), respectively, with a release medium of 20 mL PBS (pH 7.4, containing 0.2% Tween-80). The release study was conducted at 37 °C and a speed of 150 rpm on a shaker (Zhichu, ZQTY-70/ZHTY-70, Shanghai, China). The amount of quercetin released from Q@MPDA was determined by HPLC (1260 Infinity, Agilent technologies, USA). The chromatographic conditions were as follows. Agilent-C18 column (250 mm × 4.6 mm, 5 μm); mobile phase: 0.1% phosphoric acid in water/acetonitrile (55:45, *v/v*); flow rate: 1 ml/min; detection wavelength: 375 nm.

2.4. Cell cytotoxicity study

The L929, BMDM, and BMSC were seeded into the 96-well plates at a density of 5×10^3 per well. The cells were incubated with Q or MPDA at different concentrations for 24 h. The cell viability was measured using a CCK8 method and detected by a microplate reader (Agilent, BioTek Synergy H1, Santa Clara, USA) at 450 nm.

2.5. Hemolysis assay

SD Rat red blood cells (2%) and Q@MPDA were co-incubated in PBS at 37 °C for 30 min, and after centrifugation, the medium was spectrophotometrically measured at 545 nm. The hemolysis rate was quantified by comparing it to the control group (H_2O treatment) as in Eq. (1):

$$\text{Hemolysis rate (\%)} = (\text{Sample absorbance} - \text{Control absorbance}) / (\text{Complete lysis absorbance} - \text{Control absorbance}) \times 100 \quad (1)$$

2.6. Macrophage uptake study and morphology observation

Coumarin-6-labeled MPDA (50 ng/mL) was incubated with pro-inflammatory M1Φ (BMDM) for 4 h and washed three times with PBS. The cells were fixed with 4% paraformaldehyde, stained with DAPI (1 μg/mL), and observed under a fluorescent microscope (ZEISS, CARL, Oberkochen, Germany). Mean fluorescence intensity was also measured using flow cytometry (Agilent, NovoCyte, Santa Clara, USA). Mature macrophages were induced to become pro-inflammatory M1Φ and anti-inflammatory M2Φ in the 24-well plates, and then treated with quercetin (30 μmol/L) or Q@MPDA (with an equal quercetin concentration) for 24 h. The macrophage morphology was observed and captured using a microscope after treatment.

2.7. Effects of Q@MPDA on pro-inflammatory macrophage repolarization, and anti-inflammatory activities

BMDMs and gingival tissues were collected after treatment. RNA was extracted, reverse-transcribed to cDNA, and analyzed using primers listed in Supporting Information Table S1. MΦ phenotype was determined by flow cytometry (FCM) and Western blotting, using antibodies listed in Supporting Information Tables S2 and S3. The concentration of cytokines secrNCMeted by the macrophages in the culture medium supernatant was measured by ELISA kits.

The ligature-induced periodontitis model was established in the male C57BL/6 mice (7−8 weeks old). They were randomly divided into 4 groups ($n = 3$): normal mice (N), 10 μL P.g-LPS intragingival injection (PD), 10 μL quercetin (1 mg/mL) intragingival injection (Q), and 10 μL Q@MPDA intragingival injection (MQ). Immunofluorescence and immunohistochemistry were performed to detect pro-inflammatory cytokines in gingival tissue, using antibodies listed in Supporting Information Table S4. Maxillaries were harvested and analyzed by histology (H&E staining) and Masson staining to evaluate inflammation. Micro-CT (BRUKER, SkyScan1176, Karlsruhe, Germany) and three-dimensional reconstruction were used to evaluate alveolar bone resorption. The distance from the cemento-enamel junction (CEJ) to the alveolar bone crest (ABC) for the maxillary first and second molars was measured to assess periodontal bone loss. Methylene Blue hydrate staining was used to observe maxillaries under microscopy (LEICA, S8AP0, Shanghai, China). Finally, the heart, liver, spleen, lung, and kidney were obtained for pathological examination.

2.8. Detection of ROS scavenging activity of Q@MPDA

To detect intracellular ROS scavenging abilities, BMDMs were stimulated with 1 μg/mL LPS for 6 h, and then treated with either quercetin or Q@MPDA for 2 h, and finally incubated with DCFH-

DA for 30 min. FCM and fluorescence microscope were used for analysis. The ROS scavenging effect of quercetin and Q@MPDA was evaluated using an animal imaging system (IVIS SPECTRUM, PERKIN ELMER, Boston, USA). C57BL/6 mice ($n = 3$) were intragingivally injected with LPS (1 mg/mL, 5 μL) per day for four days, followed by daily intragingival administration of 5 μL Q or Q@MPDA at 2 mg/mL quercetin concentration. Positive and negative controls were LPS-injected mice without and with treatment, respectively. After four days, DCFH-DA (3.6 mg/kg, i.p.) was injected and ROS levels were detected using fluorescence imaging (excitation filter: 440−510 nmf; emission filter: 490−520 nm long pass). The remaining ROS was quantified to evaluate scavenging capacity.

2.9. *Mitochondrial related assays*

Intracellular mitochondria were labeled with MitoTracker Red CMXRos dye and detected using FCM and laser confocal microscopy (ZEISS, CARL, Oberkochen, Germany). Intracellular mtROS levels were measured using MitoSOX™ Red mitochondrial superoxide

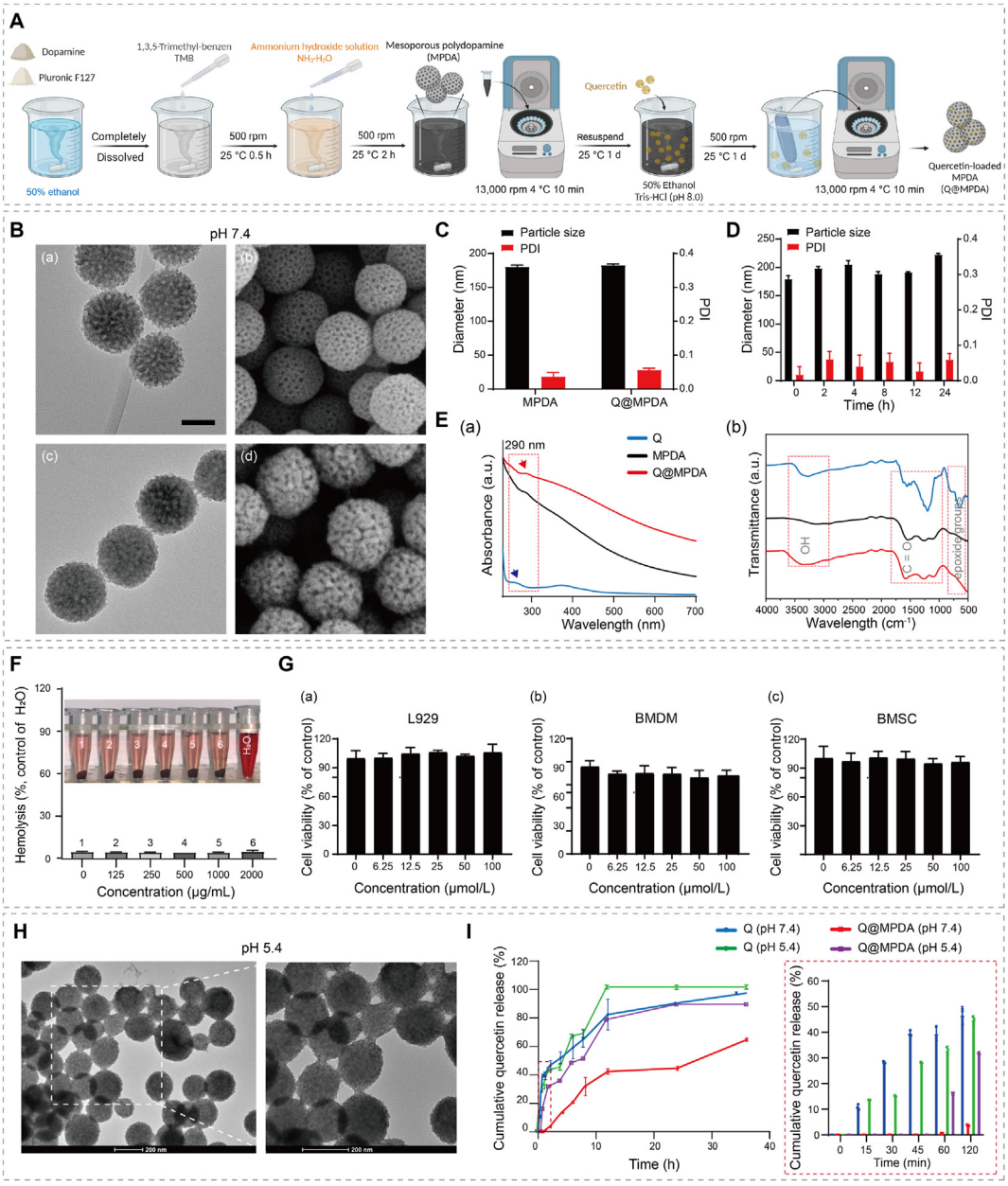

Figure 1 Characterization of MPDA and Q@MPDA. (A) Schematic diagram of MPDA and Q@MPDA preparation process. (B) TEM images of MPDA (a) and Q@MPDA (c), and SEM images of MPDA (b) and Q@MPDA (d) (scale bar: 100 nm). (C) Hydrodynamic size and PDI. (D) Particle size change in artificial saliva. (E) The spectra of UV−Vis (a) and FTIR (b). (F) Hemolysis assessment of Q@MPDA. (G) Cell viability assay of L929, BMDM, and BMSC incubated with Q@MPDA. (H) TEM images of MPDA in an acidic environment (pH 5.4). (I) Drug release profiles of quercetin from Q@MPDA within 36 h (insert: drug release within 120 min). Mean ± SD, $n = 3$.

indicator *via* FCM and CLSM. To investigate the role of mitochondrial function in macrophage polarization, oligomycin A (5 mmol/L) was used to induce mitochondrial dysfunction, and JC-1 was used to indicate mitochondrial membrane potential, observed *via* fluorescence microscopy. Changes in cytokine concentration were detected *via* Western blotting, qPCR, and analysis of cell supernatants.

2.10. Osteogenesis effect

BMSCs were seeded at a density of 1×10^5 cells/mL in the 24-well plates and cultured with osteogenic induction solution, complete DMEM medium, pro-inflammatory M1Φ supernatant, anti-inflammatory M2Φ supernatant, Q-treated cell supernatant, and Q@MPDA-treated cell supernatant. After three days, intracellular ALP expression was detected using the BCIP/NBT Alkaline Phosphatase Color Development Kit.

2.11. Statistical analysis

The data were presented as mean ± SD deviation and analyzed using SAS system. All data are analyzed by *T*-test (between two groups) or one-way ANOVA (between multiple groups). Statistical significance was denoted as $^*P < 0.05$, $^{**}P < 0.01$, $^{***}P < 0.001$.

3. Results

3.1. Characterization of Q@MPDA

The synthesis of MPDA was facile by using a one-pot method (Fig. 1A). The morphology of the quercetin-loaded MPDA (Q@MPDA) was revealed by the TEM and SEM images, showing a regular porous structure and particle size distribution (Fig. 1B).

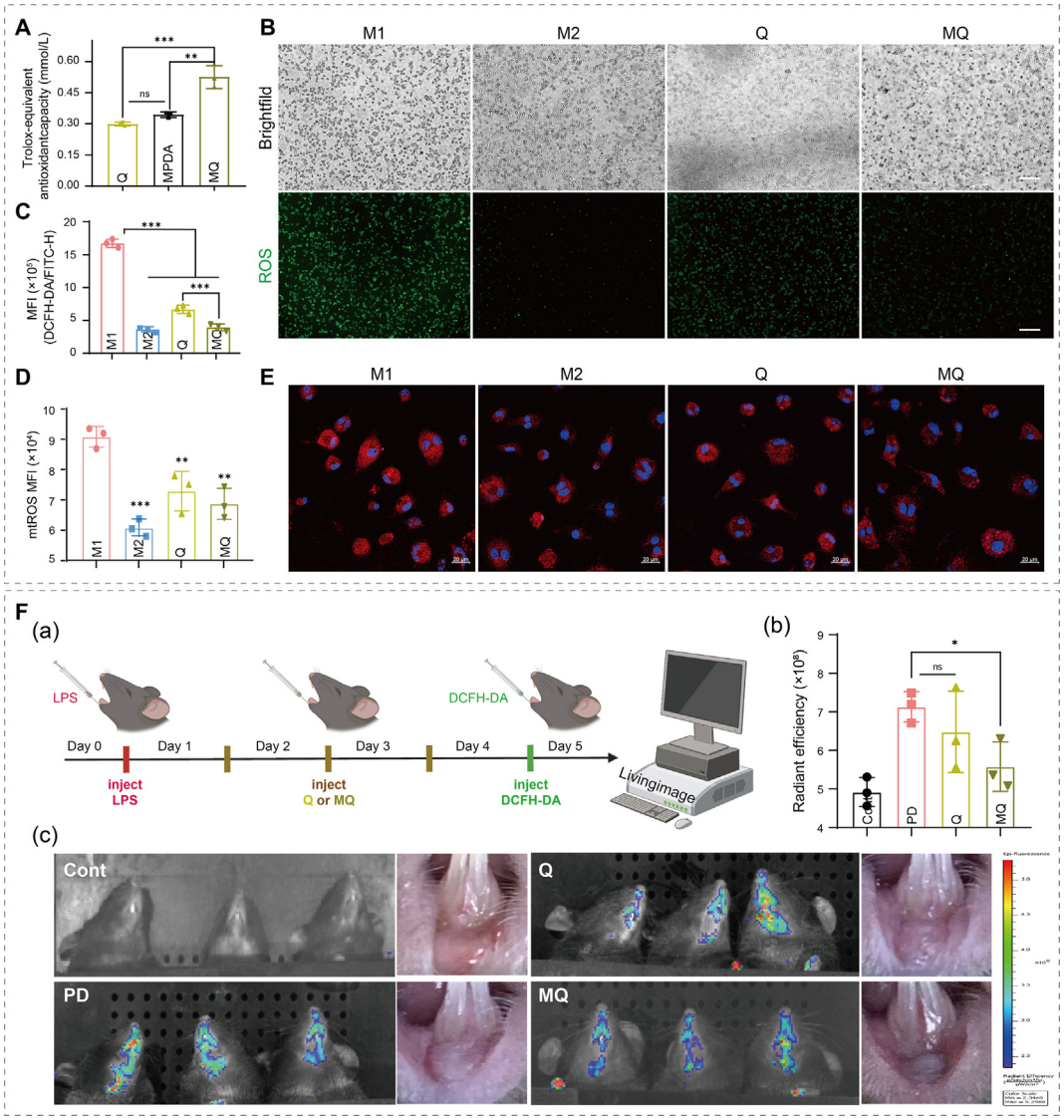

Figure 2 Anti-ROS properties of Q@MPDA. (A) Total antioxidant capacity. (B) Intracellular ROS observed by fluorescence microscopy, scale bar: 100 μm. (C) Detection of total intracellular ROS levels using flow cytometry and statistical analysis. (D) Representative image and (E) Quantified analysis of the mtROS change in BMDMs after treatment (scale bar: 20 μm). (F) (a) Schematic illustration of animal experiment design, (b) semi-quantitative analysis of fluorescence intensity, and (c) fluorescence images of ROS level in the periodontium after treatment. Mean ± SD ($n = 3$); ns, no significance, $^*P < 0.05$, $^{**}P < 0.01$, $^{***}P < 0.001$.

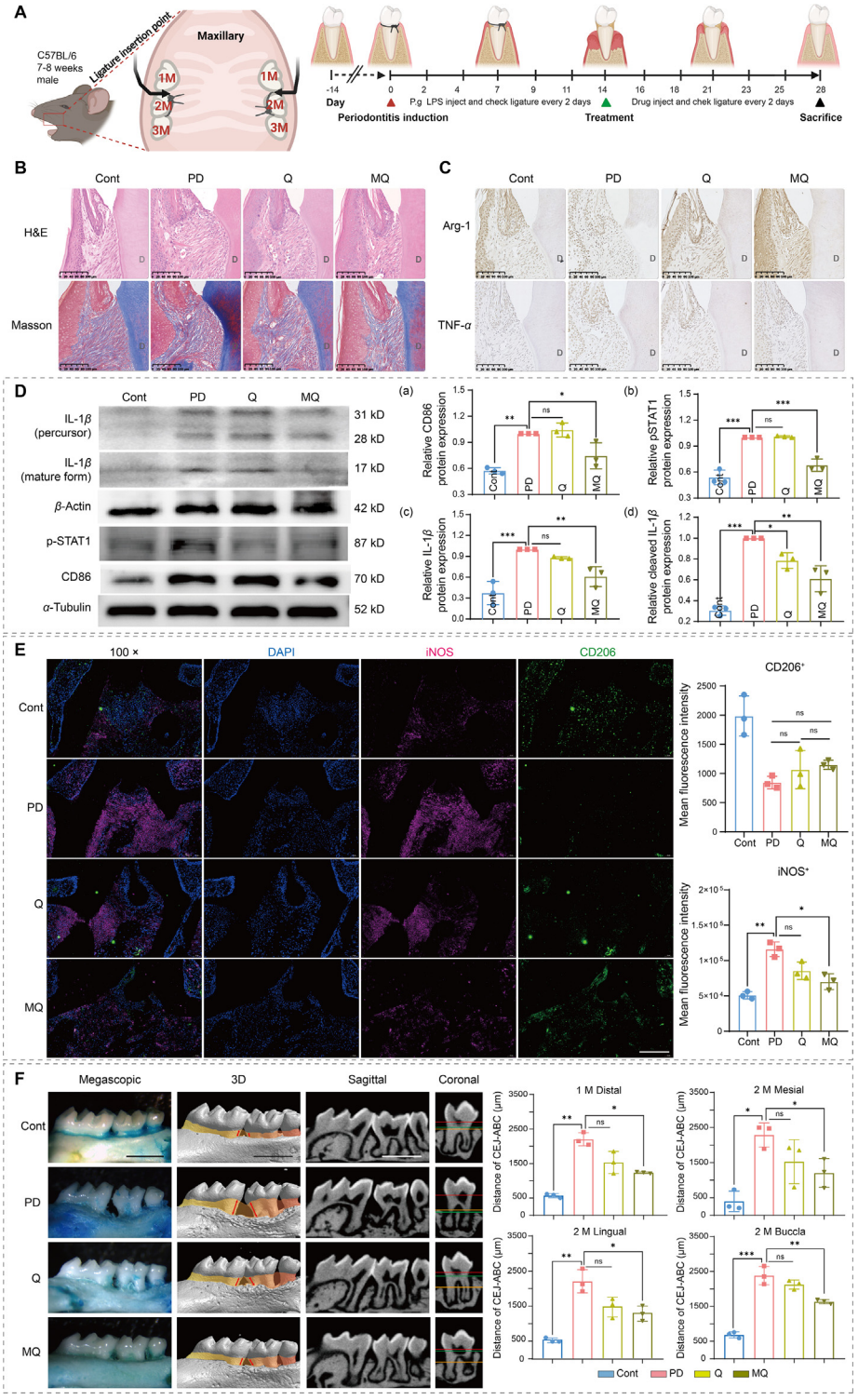

Figure 3 Q@MPDA alleviates inflammation and alveolar bone loss in periodontitis mice. (A) Schematic illustration of study design. (B) H&E and Masson staining of the periodontium slices. (C) Pro-inflammatory macrophages in the gingiva detected by IHC. (D) WB images of gingiva show pro-inflammatory macrophages and statistical analysis. (E) IFC images indicate anti-inflammatory macrophages and pro-inflammatory macrophages in the gingiva (blue: DAPI, green: CD206, pink: iNOS, scale bar: 100 μm) and statistical analysis. (F) The images of maxillary molar areas and the analysis of the CEJ-ABC linear distance (red line: CEJ; green line: the buccal ABC. yellow line: the palatal ABC. Scale bar: 3 mm). Cont: the group was received PBS only. PD: the group was ligatured and intragingivally injected with P.g LPS. Q: tooth ligatured + intragingival injected P.g LPS + 10 μg quercetin, a total of 6 times. MQ: tooth ligatured + intragingival injected P.g LPS + 10 μg Q@MPDA, a total of 6 times. 1M: maxillary first molar; 2M: maxillary second molar; 3M: maxillary third molar. Mean ± SD, ($n = 3$); ns, no significance, $^{*}P < 0.05$, $^{**}P < 0.01$, $^{***}P < 0.001$.

The average hydrodynamic diameters of MPDA and Q@MPDA were180.3 nm and 182.7 nm (Fig. 1C, Supporting Information Table S5), with a polydispersity of 0.04 and 0.06, respectively. Their zeta potential was −35.2 and −38.4 mV, respectively (Table S5). Both Q@MPDA and MPDA remained stable in the artificial saliva at 37 °C for 24 h (Fig. 1D). The DL% and EE% of Q@MPDA were 39.3% and 7.0%, respectively (Supporting Information Table S6). The nitrogen plot exhibited a type-IV isotherm indicative of both MPDA and Q@MPDA (Supporting Information Fig. S1).

The UV−Vis spectra of quercetin, MPDA, and Q@MPDA were measured and shown in Fig. 1Ea. Free quercetin showed two

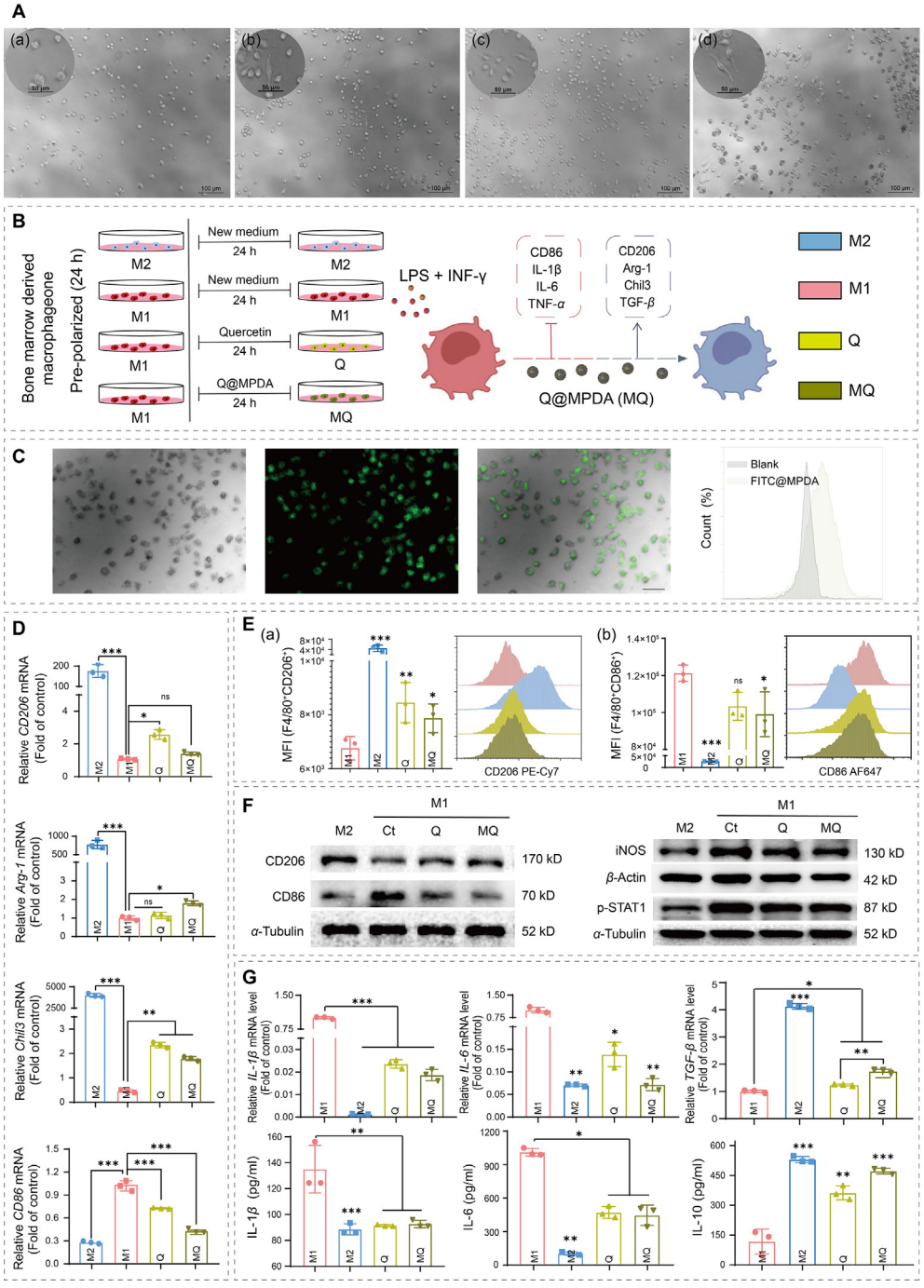

Figure 4 Q@MPDA promotes the switch from pro-inflammatory M1 macrophages toward anti-inflammatory M2 macrophages. (A) Cell morphology after treatment. (a) M1, (b) M2, (c) quercetin-treated M1, and (d) Q@MPDA-treated M1. (B) Schematic illustration of experimental design. (C) Fluorescence images of BMDMs after incubation with Coumarin-6-loaded MPDA (scale bar, 100 μm). (D) The mRNA expression levels of *CD86*, *CD206*, *Arg-1*, and *Chil3*. (E) Flow cytometry histogram and quantitation analysis of CD86 (a) and CD206 (b). (F) M2 and M1 phenotypes detected by Western blotting. (G) Inflammation-relative cytokine mRNA and protein expression levels in BMDMs. M2: M2 phenotype macrophages; M1: M1 phenotype macrophages; Q: M1 macrophages treated with quercetin; MQ: M1 macrophages treated with Q@MPDA. Mean ± SD, $n = 3$; ns, no significance, $^{*}P < 0.05$, $^{**}P < 0.01$, $^{***}P < 0.001$.

absorption bands (blue curve): Band I (350−380 nm) and Band II (240−260 nm), which are related to the cinnamoyl and benzoyl groups, respectively. MPDA (blank curve) showed a catechol absorption peak at about 290 nm clearly. The spectrum of Q@MPDA (red curve) showed both the MPDA and quercetin absorption peaks. Notably, there was a decrease in the intensity of the quercetin-related chromophore (hyperchromatic shift with λ_{max2} of 370 nm). The FTIR spectra (Fig. 1Eb) revealed an absorption band of quercetin at 1055 cm^{-1} (alkoxy), and a new peak at 1110 cm^{-1} in Q@MPDA, which may be due to the stretching vibration of C−N bonding and deformation vibration of −N−H bonding[16]. The disappearance of the 970 and 1223 cm^{-1} of the epoxide groups in the Q@MPDA indicated an interaction between the epoxide groups of quercetin and the amine groups of MPDA[17]. One distinct peak of Q@MPDA appeared at 3353 cm^{-1}, corresponding to the characteristic absorption peak of the phenolic hydroxy group of quercetin[8], which confirmed the loading of quercetin on MPDA.

Q@MPDA exhibited good biocompatibility, with the hemolysis rate remaining under 6% even at a high dose of 2 mg/mL (Fig. 1F) and the cell viability remaining above 80% at a dose of 100 μg/mL in various cell types (L929, BMDM, and BMSC) (Fig. 1G).

The drug release behavior of Q@MPDA was studied. Acidic conditions promoted MPDA degradation (Fig. 1H), and the release of quercetin was accelerated at pH 5.4, while sustained release of quercetin was observed over 36 h at pH 7.4 (Fig. 1I).

3.2. *ROS-reducing capacity of Q@MPDA*

Supporting Information Fig. S2 indicates that quercetin effectively reprogrammed M1 macrophages at a concentration of 30 μmol/L, which thereby was selected for subsequent experiments. The antioxidant capability of Q@MPDA was approximately two-fold higher than other groups (Fig. 2A). Our results also showed that Q@MPDA reduced the intracellular ROS levels (Fig. 2B and C), and especially the mtROS levels (Fig. 2D and E). ROS is a second messenger that drives inflammation, and its change can be used an indicator of inflammation status. Furthermore, Q@MPDA treatment could significantly reduce ROS in the inflamed gingiva (Fig. 2F).

3.3. *Ameliorating periodontium inflammation and alveolar bone resorption by Q@MPDA*

The periodontitis treatment was carried out (Fig. 3A) and the periodontal tissues were collected to assess the effectiveness of inflammation relief and tissue repair at the endpoint. The histological analysis, including H&E staining and Masson staining, revealed a high level of inflammatory cell infiltration and disorganized periodontal fibers in the periodontitis model group (Fig. 3B). The immunohistochemistry (IHC) (Fig. 3C), Western blot (WB) (Fig. 3D), and immunofluorescence (IF) (Fig. 3E) results demonstrated the effective treatment with Q@MPDA, evidenced by a significant decrease in pro-inflammatory macrophages. Accordingly, the pro-inflammatory cytokines IL-1β (Fig. 3D) and TNF-α (Fig. 3C) were also reduced in the gingiva after treatment with Q@MPDA. Furthermore, the alveolar bone resorption was alleviated (Fig. 3F), but there was no significant difference between quercetin and Q@MPDA.

3.4. *Macrophage repolarization from M1 to M2 and inflammation attenuation by Q@MPDA*

After Q@MPDA treatment, the morphology of macrophages was changed, shifting from a large, round shape (M1-type) to an elongated, shuttle-like shape (M2-type) (Fig. 4A). To further confirm the drug's efficacy, we administered quercetin to stimulate M1 macrophages (Fig. 4B). Macrophages could efficiently take up the liposomes within 4 h (Fig. 4C). The qPCR results revealed downregulation of the M1 marker *CD86*, and upregulation of the M2 markers *CD206*, *Arg-1*, and *Chill3* after treatment (Fig. 4D). The repolarization from M1 to M2 mediated by Q@MPDA treatment was further demonstrated by the protein expression of the related biomarkers (CD206, CD86) (Fig. 4E and F).

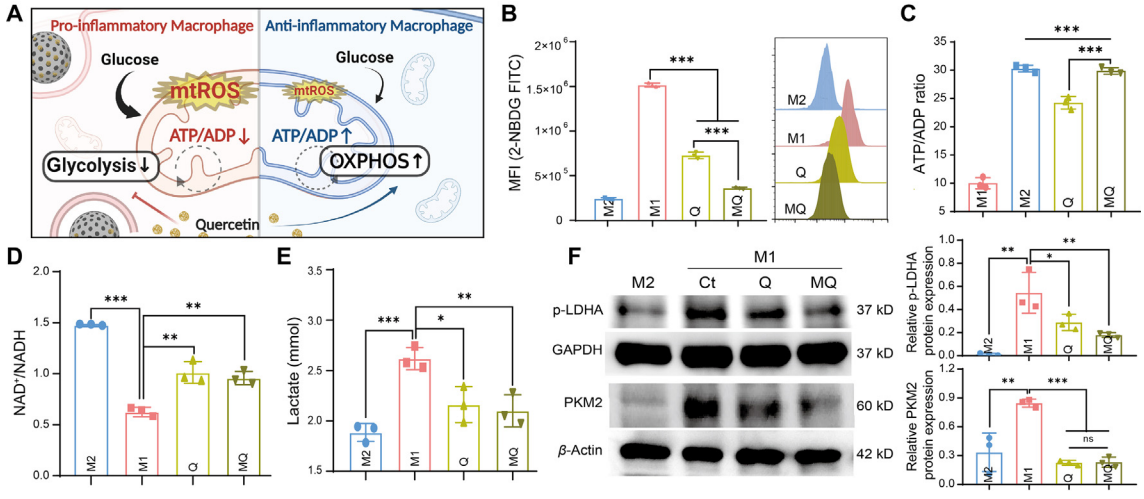

Figure 5 Q@MPDA attenuates the excess ROS production of pro-inflammatory M1 macrophages and rectifies the perturbed mitochondrial state. (A) Schematic illustration of the mechanism. (B) 2-NBDG uptake by macrophages. (C) The ratio of ATP/ADP after 12 h of stimulation. (D) The levels of NAD^+/NADH expression. (E) The levels of lactate secretion from macrophage. (F) p-LDHA and PKM2 western blotting images and their analysis. M2: M2 macrophages; M1: M1 macrophages; Q: M1 macrophages treated with quercetin; MQ: M1 macrophages treated with Q@MPDA. Mean ± SD, (n = 3); *P < 0.05, **P < 0.01, ***P < 0.001.

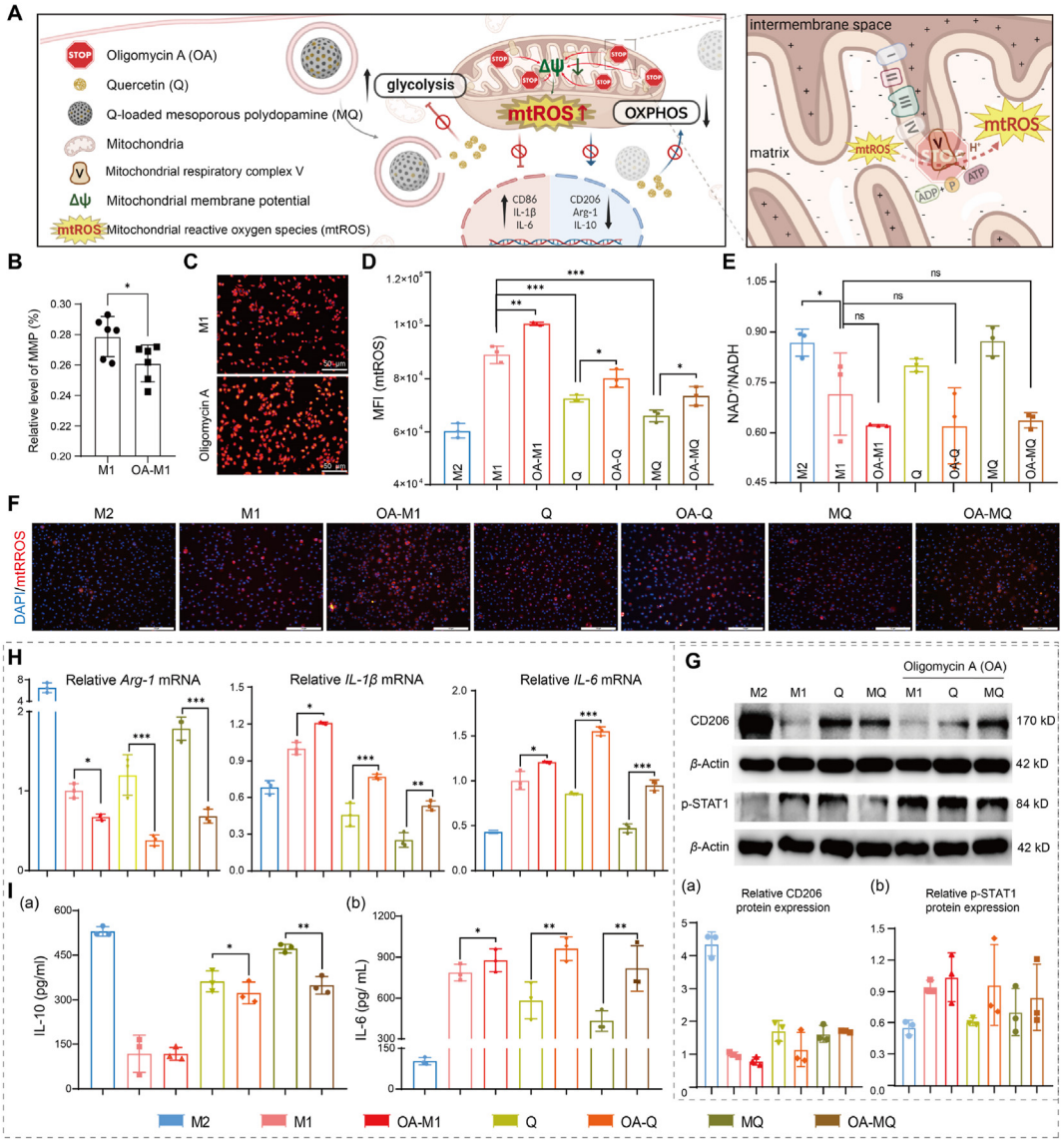

Figure 6 Inhibition of OXPHOS counteracts the effect of Q@MPDA on regulating macrophages. (A) Schematic diagram of the mechanism. The change of mitochondrial membrane potential (B) and mitochondrial ROS (C) of pro-inflammatory macrophages after giving Oligomycin A (OA). (D) Quantitation analysis of mitochondrial ROS by flow cytometry. (E) The levels of NAD^+/NADH expression. (F) The fluorescence images of mitochondrial ROS (scale bar, 100 μm). (G) RNA expression levels of *Arg-1* (a), *IL-1β* (b), and *IL-6* (c). (H) ELISA of IL-10 (a) and IL-6 (b). (I) Cytokine levels of macrophages. M2: M2 macrophages; M1: M1 macrophages; OA-M1: M1 macrophages incubated with 5 μmol/L OA; Q: M1 macrophages treated with quercetin; OA-Q: M1 macrophages simultaneously treated with OA and quercetin; MQ: M1 macrophages treated with Q@MPDA; OA-MQ: M1 macrophage simultaneously treated with OA and Q@MPDA. Mean ± SD, $n = 3$. $^{**}P < 0.01$, $^{***}P < 0.001$.

Furthermore, the inflammatory cytokines *IL-1β* and *IL-6* were upregulated, whereas the anti-inflammatory *TGF-β* downregulated at a mRNA level. The secreted IL-1β and IL-6 contents in the cell supernatant were also reduced, while IL-10 was elevated (Fig. 4G). These results indicated that Q@MPDA was able to reprogram pro-inflammatory M1 macrophages to an anti-inflammatory M2 phenotype.

3.5. *Inhibiting glucose uptake and lactate production in macrophages by Q@MPDA*

To assess glucose uptake by macrophages, we employed 2-NBDG (a fluorescent derivative of glucose) for monitoring intracellular glucose uptake. Flow cytometry analysis revealed a reduction in glucose uptake following Q@MPDA treatment (Fig. 5B). Moreover, the ATP/ADP ratio (Fig. 5C) and the NAD^+/NADH ratio (Fig. 5D) in inflammatory macrophages also increased, suggesting the diminished intracellular energy production.

The secretion of lactate, the end product of glycolysis, was reduced following quercetin or Q@MPDA treatment (Fig. 5E). Lactate dehydrogenase A (LDHA), a key enzyme associated with lactic acid production, was down-regulated (Fig. 5F). Pyruvate kinase isozymes M2 (PKM2), responsible for catalyzing the inter-conversion of pyruvate and lactate *via* NADH and NAD^+ conversion to producing ATP, were also down-regulated (Fig. 5F). Based on the above

results, we concluded that Q@MPDA reversed the macrophage phenotype by regulating macrophage glycolysis (Fig. 5A).

3.6. *The antioxidant capacity of Q@MPDA and OXPHOS*

In normal macrophages, glycolysis and OXPHOS work in homeostasis, with reduced glycolysis leading to increased OXPHOS, and vice versa. To examine the role of OXPHOS in antioxidation in macrophages, we used oligomycin A (OA) which can inhibit ATP synthase to inhibit OXPHOS (Fig. 6A), and the results showed the mitochondrial hyperpolarization and elevated intracellular mitochondrial membrane potential (Fig. 6B) and the mtROS level (Fig. 6C). The suppressing OXPHOS led to the elevated level of mtROS (Fig. 6D and F, and Supporting Information Fig. S3) and the decreased ratio of NAD^+/NADH (Fig. 6E) in the macrophages. It indicated the suppressing OXPHOS promoted the induction of pro-inflammatory phenotype (M1).

Furthermore, the repolarizing effect of Q@MPDA on inflammatory M1 macrophages was attenuated by inhibition of OXPHOS using OA. Compared to Q@MPDA treatment alone, Q@MPDA and OA co-administration exhibited higher pro-inflammatory IL-6 and lower anti-inflammatory IL-10 levels (Fig. 6H). Accordingly, the PCR results also revealed that OA attenuated the M2 polarization effect of Q@MPDA, showing the decreased *Arg-1* (M2-associated gene, Fig. 6Ga), but increasing the M1-associated *IL-1β* and *IL-6* gene levels (Fig. 6Gb and c). This suggests that the metabolism reprogramming from glycolysis to OXPHOS played an important role in Q@MPDA treatment. It should be noted that western blotting results and semi-quantitative analysis showed a similar trend (CD206 and p-STAT1) (Fig. 6I).

4. Discussions

In the context of periodontitis, inflammatory phenotypic changes in macrophages are important for driving disease progression[6,18]. To address this, we designed a Q@MPDA system for delivering quercetin to inflammatory macrophages in periodontitis. By making use of the adhesive properties of MPDA, we overcome the challenge of salivary washout and achieve intragingival retention of quercetin. Q@MPDA treatment significantly inhibited soft tissue inflammation, reduced inflammatory cytokines such as TNF-α and IL-1β, and exhibited organized fibers. Additionally, Q@MPDA treatment led to a decrease in alveolar bone resorption, aligning with clinical report linking elevated TNF-α and IL-1β in gingival crevicular fluid to alveolar bone resorption[19,20]. Furthermore, the *in vivo* results demonstrated that Q@MPDA effectively decreased ROS in the periodontal tissues. ROS are inflammatory substances that cause damage to the periodontal tissue, and the removal of excessive ROS is crucial for maintaining healthy conditions of periodontal tissues[21,22].

The mechanisms underlying how Q@MPDA promotes the repolarization of inflammatory macrophages remain unclear. Previous studies demonstrated that quercetin could inhibit glycolysis[23]. Importantly, altering glucose metabolism can induce macrophage repolarization[4]. For example, increased glycolysis could induce high levels of ROS in macrophages and promote M1 polarization[1]. Our strategy was to apply Q@MPDA to inhibit glycolysis in inflammatory macrophages, leading to increased OXPHOS and decreased ROS, thus switching to an anti-inflammatory state, thus revealing a potential therapeutic avenue *via* immunometabolic regulation.

Q@MPDA therapy significantly reduced total cellular ROS and mitochondria ROS, suggesting that mitochondria could be a target of Q@MPDA. In addition, Q@MPDA treatment increased glucose utilization in macrophages by promoting OXPHOS, as evidenced by an increase in ATP/ADP and NAD^+/NADH ratios, but a decrease in lactate production. Accordingly, OXPHOS inhibition by OA can counteract the effect of Q@MPDA on macrophage repolarization from M1 to M2. Our findings were consistent with the previous studies[24,25], and indicated an important role of OXPHOS in M2 polarization.

5. Conclusions

In this study, we implemented MPDA as a bio-adhesive carrier for quercetin intragingival delivery to improve its local retention and efficacy. Our results demonstrated that quercetin-loaded MPDA effectively modulates macrophage phenotype in the periodontium, leading to the relief of inflammation. The mechanistic investigations revealed that quercetin exerts anti-inflammatory effects by inhibiting glycolysis in M1-type macrophages and promoting OXPHOS to decrease intracellular mtROS content. This work provides an immunometabolic strategy for effective periodontitis treatment using MPDA-encapsulating quercetin that is a common dietary compound, with a benefit of safety for long-term use.

Acknowledgments

The study was supported by the National Key Research and Development Program of China (2022YFE0203600, China), National Nature Science Foundation of China (82271028, 82341232), the Department of Science and Technology of Guangdong Province (High-level New R&D Institute 2019B090904008, High-level Innovative Research Institute 2021B0909050003, China), and Zhongshan Municipal Bureau of Science and Technology (LJ2021001 & CXTD2022011, China). It also supported by the Project of Biobank (YBKB202102, China), the Research Discipline Fund (KQYJXK2020, China), the Cross-disciplinary Research Fund (JYJC202205, China) from Shanghai Ninth People's Hospital (SHSMU-ZDCX20212500, China), and the Shanghai Pujiang Program (22PJD038, China). Images in Graphic Abstract and Fig. 1A, 2F and 3A, 4B, 5A, 6A, S2 created with BioRender.com. We thank the Large-scale Protein Preparation System at the National Facility for Protein Science in Shanghai (NFPS), Shanghai Advanced Research Institute, Chinese Academy of Sciences for providing technical support and assistance in data collection and analysis. Special thanks are extended to the insightful discussions and contributions from Yuge Zhao, Li Long, and Jiaxin Zhang.

Author contributions

Yi Zhang: investigation, conceptualization, methodology, data curation, formal analysis, writing, review and editing, visualization. Junyu Shi: resources, review, and editing. Jie Zhu: participated part of the experiments. Xinxin Ding, Jianxu Wei, Xue Jiang and Yijie Yang: Formal analysis. Xiaomeng Zhang: supervision, review, and editing. Yongzhuo Huang: supervision, resources, writing, review and editing, funding acquisition. Hongchang Lai: supervision, resources, funding acquisition. All the authors have read and approved the final manuscript.

Conflicts of interest

The authors have no conflicts of interest to declare.

Appendix A. Supporting information

Supporting information to this article can be found online at https://doi.org/10.1016/j.apsb.2024.07.008.

References

1. Mills EL, Kelly B, Logan A, Costa ASH, Varma M, Bryant CE, et al. Succinate dehydrogenase supports metabolic repurposing of mitochondria to drive inflammatory macrophages. *Cell* 2016;**167**:457–70.e13.
2. Mouton AJ, Li X, Hall ME, Hall JE. Obesity, hypertension, and cardiac dysfunction: novel roles of immunometabolism in macrophage activation and inflammation. *Circ Res* 2020;**126**:789–806.
3. Duan S, Lou X, Chen S, Jiang H, Chen D, Yin R, et al. Macrophage LMO7 deficiency facilitates inflammatory injury *via* metabolic-epigenetic reprogramming. *Acta Pharm Sin B* 2023;**13**:4785–800.
4. Blagih J, Jones RG. Polarizing macrophages through reprogramming of glucose metabolism. *Cell Metab* 2012;**15**:793–5.
5. Lee HJ, Kang IK, Chung CP, Choi SM. The subgingival microflora and gingival crevicular fluid cytokines in refractory periodontitis. *J Clin Periodontol* 1995;**22**:885–90.
6. Yu T, Zhao L, Huang X, Ma C, Wang Y, Zhang J, et al. Enhanced activity of the macrophage M1/M2 phenotypes and phenotypic switch to M1 in periodontal infection. *J Periodontol* 2016;**87**:1092–102.
7. Wang F, Zhang S, Vuckovic I, Jeon R, Lerman A, Folmes CD, et al. Glycolytic stimulation is not a requirement for M2 macrophage differentiation. *Cel Metab* 2018;**28**:463–75.e4.
8. Wang Y, Li C, Wan Y, Qi M, Chen Q, Sun Y, et al. Quercetin-loaded ceria nanocomposite potentiate dual-directional immunoregulation *via* macrophage polarization against periodontal inflammation. *Small* 2021;**17**:e2101505.
9. Wei Y, Fu J, Wu W, Ma P, Ren L, Yi Z, et al. Quercetin prevents oxidative stress-induced injury of periodontal ligament cells and alveolar bone loss in periodontitis. *Drug Des Devel Ther* 2021;**15**:3509–22.
10. Hu M, Song HY, Chen L. Quercetin acts *via* the G3BP1/YWHAZ axis to inhibit glycolysis and proliferation in oral squamous cell carcinoma. *Toxicol Mech Methods* 2023;**33**:141–50.
11. Zhao P, Wang S, Jiang J, Gao Y, Wang Y, Zhao Y, et al. Targeting lactate metabolism and immune interaction in breast tumor *via* protease-triggered delivery. *J Control Release* 2023;**358**:706–17.
12. Zhu J, Wang R, Yang C, Shao X, Zhang Y, Hou J, et al. Blocking tumor-platelet crosstalk to prevent tumor metastasis *via* reprograming glycolysis using biomimetic membrane-hybridized liposomes. *J Control Release* 2024;**366**:328–41.
13. Liu Y, Ai K, Lu L. Polydopamine and its derivative materials: synthesis and promising applications in energy, environmental, and biomedical fields. *Chem Rev* 2014;**114**:5057–115.
14. Maridas DE, Rendina-Ruedy E, Le PT, Rosen CJ, et al. Isolation, culture, and differentiation of bone marrow stromal cells and osteoclast progenitors from mice. *J Vis Exp: JoVE* 2018;**131**:56750. 6.
15. Long L, Xiong W, Lin F, Hou J, Chen G, Peng T, et al. Regulating lactate-related immunometabolism and EMT reversal for colorectal cancer liver metastases using shikonin targeted delivery. *J Exp Clin Cancer Res* 2023;**42**:117.
16. Liu Y, Fan Q, Huo Y, Liu C, Li B, Li Y. Construction of a mesoporous polydopamine@GO/cellulose nanofibril composite hydrogel with an encapsulation structure for controllable drug release and toxicity shielding. *ACS Appl Mater Inter* 2020;**12**:57410–20.
17. Cui W, Li M, Liu J, Wang B, Zhang C, Jiang L, et al. A strong integrated strength and toughness artificial nacre based on dopamine cross-linked graphene oxide. *ACS Nano* 2014;**8**:9511–7.
18. Luan J, Li R, Xu W, Sun H, Li Q, Wang D, et al. Functional biomaterials for comprehensive periodontitis therapy. *Acta Pharm Sin B* 2023;**13**:2310–33.
19. Kim JY, Kim KR, Kim HN. The potential impact of salivary IL-1 on the diagnosis of periodontal disease: a pilot study. *Healthc (Basel)* 2021;**9**:729.
20. Tani-Ishii N, Tsunoda A, Teranaka T, Umemoto T. Autocrine regulation of osteoclast formation and bone resorption by IL-1 alpha and TNF alpha. *J Dent Res* 1999;**78**:1617–23.
21. Shi L, Ji Y, Zhao S, Li H, Jiang Y, Mao J, et al. Crosstalk between reactive oxygen species and dynamin-related protein 1 in periodontitis. *Free Radic Biol Med* 2021;**172**:19–32.
22. Sczepanik FSC, Grossi ML, Casati M, Goldberg M, Glogauer M, Fine N, et al. Periodontitis is an inflammatory disease of oxidative stress: we should treat it that way. *Periodontol 2000* 2020;**84**:45–68.
23. Wang L, Ji S, Liu Z, Zhao J. Quercetin inhibits glioblastoma growth and prolongs survival rate through inhibiting glycolytic metabolism. *Chemotherapy* 2022;**67**:132–41.
24. Wculek SK, Heras-Murillo I, Mastrangelo A, Mananes D, Galan M, Miguel V, et al. Oxidative phosphorylation selectively orchestrates tissue macrophage homeostasis. *Immunity* 2023;**56**:516–30.e9.
25. Baseler WA, Davies LC, Quigley L, Ridnour LA, Weiss JM, Hussain SP, et al. Autocrine IL-10 functions as a rheostat for M1 macrophage glycolytic commitment by tuning nitric oxide production. *Redox Biol* 2016;**10**:12–23.